Nonlinear error-field penetration in low density ohmically heated tokamak plasmas



2012 Plasma Phys. Control. Fusion 54 094002

(http://iopscience.iop.org/0741-3335/54/9/094002)

Plasma Phys. Control. Fusion **54** (2012) 094002 (12pp) doi:10.1088/0741-3335/54/9/094002

# Nonlinear error-field penetration in low density ohmically heated tokamak plasmas

**R Fitzpatrick**

Institute for Fusion Studies, Department of Physics, University of Texas at Austin, Austin, TX 78712, USA

E-mail: rfitzp@farside.ph.utexas.edu

Received 1 December 2011, in final form 6 March 2012
Published 17 August 2012
Online at stacks.iop.org/PPCF/54/094002

**Abstract**

A theory is developed to predict the error-field penetration threshold in low density, ohmically heated, tokamak plasmas. The novel feature of the theory is that the response of the plasma in the vicinity of the resonant surface to the applied error-field is calculated from nonlinear drift-MHD (magnetohydrodynamical) magnetic island theory, rather than linear layer theory. Error-field penetration, and subsequent locked mode formation, is triggered once the destabilizing effect of the resonant harmonic of the error-field overcomes the stabilizing effect of the ion polarization current (caused by the propagation of the error-field-induced island chain in the local ion fluid frame). The predicted scaling of the error-field penetration threshold with engineering parameters is $(b_r/B_T)_{crit} \sim n_e\, B_T^{-1.8}\, R_0^{-0.25}$, where $b_r$ is the resonant harmonic of the vacuum radial error-field at the resonant surface, $B_T$ the toroidal magnetic field-strength, $n_e$ the electron number density at the resonant surface and $R_0$ the major radius of the plasma. This scaling—in particular, the linear dependence of the threshold with density—is consistent with experimental observations. When the scaling is used to extrapolate from JET to ITER, the predicted ITER error-field penetration threshold is $(b_r/B_T)_{crit} \sim 5 \times 10^{-5}$, which just lies within the expected capabilities of the ITER error-field correction system.

## 1. Introduction

Tokamak [1] plasmas are highly sensitive to externally generated, static, helical magnetic perturbations [2–8]. Such perturbations, which are conventionally termed error-fields, are present in all tokamak experiments because of imperfections in magnetic field-coils. An error-field can drive magnetic reconnection in an otherwise tearing-stable plasma, giving rise to the formation of locked (i.e. non-rotating) magnetic island chains at (internal) resonant magnetic flux-surfaces [9]. Such chains, which are generally known as locked modes, severely degrade global energy confinement [10], and often trigger major disruptions [2–4]. Fortunately, the (highly sub-Alfvénic) toroidal rotation that occurs naturally in all tokamak plasmas affords them some level of protection against locked mode formation. To be more exact, rotation induces localized shielding currents at the various resonant surfaces within the plasma, and these currents suppress error-field driven magnetic reconnection. Unfortunately, the residual magnetic reconnection at the resonant surfaces produces a toroidal electromagnetic locking torque that slows the plasma rotation. Moreover, the rotation is suddenly arrested once the error-field amplitude exceeds a certain critical value, permitting locked mode formation to proceed without further hinderance [11, 12]. This scenario is generally referred to as error-field penetration. The critical resonant error-field amplitude required to trigger penetration can be as small as $10^{-4}$ of the equilibrium toroidal field-strength.

Error-field penetration in low density, ohmically heated, startup plasmas often leads to unacceptable limitations on the available operating space in tokamak experiments. The scaling of the error-field penetration threshold with engineering parameters in such plasmas (at fixed shape and $q_{95}$) is conventionally expressed in the form

$$\left(\frac{b_r}{B_T}\right)_{crit} \sim n_e^{\alpha_n}\, B_T^{\alpha_B}\, R_0^{\alpha_R}, \qquad (1)$$

 

where $b_r$ is the resonant harmonic (usually, the 2,1 harmonic) of the vacuum radial error-field at the associated resonant surface, $B_T$ is the toroidal magnetic field-strength, $n_e$ is the electron number density at the resonant surface and $R_0$ is the plasma major radius. Empirical scaling studies performed on the COMPASS-D, TEXTOR, ALCATOR C-MOD, DIII-D and JET tokamaks [5–8] have established that $\alpha_n \simeq 1$, and that $\alpha_B$ ranges between $-2.9$ and $-0.6$. The former value for $\alpha_B$ was derived from COMPASS-D data [5], and the latter from ALCATOR C-MOD data [7]. Data from DIII-D and JET yield $\alpha_B$ values of $-1.0$ and $-1.2$, respectively [5]. The exponent $\alpha_R$ cannot be directly measured, but is inferred from dimensionless scaling arguments [13] to take the value $\alpha_R = 2\,\alpha_n + 1.25\,\alpha_B$ [5]. It follows that $\alpha_R$ lies in the range $-1.6$ to 1.25. The only aspect of the scaling with engineering parameters upon which data from all experiments are in agreement is that the scaling with the density is approximately linear. The considerable uncertainty in the value of $\alpha_B$ (and, hence, in the value of $\alpha_R$) leads to similar uncertainty in the predicted error-field penetration threshold for ITER. Indeed, extrapolation from JET [$n_e = 1.6 \times 10^{19}\,\mathrm{m}^{-3}$, $B_T = 3.5\,\mathrm{T}$, $R_0 = 2.95\,\mathrm{m}$, $(b_r/B_T)_{crit} = 1.1 \times 10^{-4}$] [5] to ITER ($n_e = 2 \times 10^{19}\,\mathrm{m}^{-3}$, $B_T = 5.3\,\mathrm{T}$, $R_0 = 6.2\,\mathrm{m}$) [14] yields estimates for the ITER penetration threshold ranging from $(b_r/B_T)_{crit} = 1.3 \times 10^{-5}$ to $(b_r/B_T)_{crit} = 2.7 \times 10^{-4}$. The proposed ITER error-field correction system is designed to reduce resonant error-field levels down to $b_r/B_T \simeq 5 \times 10^{-5}$ [15]. Such a system is sufficient to prevent locked mode formation in ohmically heated plasmas according to the most optimistic estimate (i.e. the latter estimate) for the ITER penetration threshold, but not according to the most pessimistic. Clearly, it is desirable to reduce the uncertainty in these estimates. One way of achieving this goal would be to derive a plausible theoretical model that is consistent with the available experimental data. Unfortunately, this has proved to be a difficult task.

The original model of Fitzpatrick [11, 12] is based on the idea that, prior to locked mode formation, error-field driven reconnection is suppressed to such an extent that the response of the plasma in the vicinity of the resonant surface to the applied error-field can be determined from linear resistive-MHD (magnetohydrodynamical) layer theory. Moreover, in this model, the electromagnetic locking torque due to the error-field is balanced by a viscous torque due to anomalous perpendicular momentum transport. The scaling of the error-field penetration threshold predicted by the Fitzpatrick model (in the so-called visco-resistive regime) takes the form

$$\left(\frac{b_r}{B_T}\right)_{crit} \sim \beta^{-1/6}\,\nu_*^{1/6}\,\rho_*^{4/3} \sim T_i^{1/6}\,B_T^{-1}\,R_0^{-7/6} \sim B_T^{-13/15}\,R_0^{-13/12}. \quad (2)$$

Here, the first scaling is in terms of the standard dimensionless parameters, $\beta$ (the ratio of the plasma thermal energy density to the magnetic energy density), $\nu_*$ (the ratio of the electron collision frequency to the electron transit frequency) and $\rho_*$ (the ratio of the ion sound radius to the plasma major radius). Moreover, in deriving this scaling, it is assumed that the momentum confinement timescale scales like the energy confinement timescale, and that the plasma heating is purely ohmic (see section 5). The second scaling is in terms of the physics parameters, $n_e$, $T_i$ (the ion temperature at the resonant surface), $B_T$, and $R_0$, and is derived from the first scaling using $\beta \sim n_e\,T_i/B_T^2$, $\nu_* \sim n_e\,R_0/T_i^{\,2}$ and $\rho_* \sim T_i^{\,1/2}/R_0\,B_T$ (see section 5). The final scaling is in terms of the engineering parameters, $n_e$, $B_T$ and $R_0$, and is derived from the second scaling on the assumption that $\nu_* \sim \beta\,\rho_*^{2/3}$, which implies the dimensionally consistent neo-ALCATOR-like [16, 17] temperature scaling $T_i \sim B_T^{4/5}\,R_0^{1/2}$ (see section 5). Unfortunately, the scaling of the penetration threshold with engineering parameters predicted by the Fitzpatrick model exhibits no dependence on the density, and is, therefore, completely inconsistent with the previously discussed experimental data.

The model of Cole and Fitzpatrick [18] is similar to that of Fitzpatrick, except that the response of the plasma in the vicinity of the resonant surface to the applied error-field is calculated from linear drift-MHD layer theory. This is appropriate in situations in which the linear layer width is less than the ion sound radius (i.e. the ion gyroradius calculated with the electron temperature). The scaling of the error-field penetration threshold predicted by the Cole and Fitzpatrick model (in the so-called first semi-collisional regime) is

$$\left(\frac{b_r}{B_T}\right)_{crit} \sim \nu_*^{1/4}\,\rho_*^{5/4} \sim n_e^{1/4}\,T_i^{1/8}\,B_T^{-5/4}\,R_0^{-1} \sim n_e^{1/4}\,B_T^{-23/20}\,R_0^{-15/16}. \quad (3)$$

(The three different scalings have the same interpretation as before.) It can be seen that the predicted scaling with engineering parameters is an improvement on that of the Fitzpatrick model, since it does, at least, exhibit some density dependence. Unfortunately, this dependence is far too weak to account for the experimental data.

The model of Cole *et al* [19] is similar to that of Cole and Fitzpatrick, except that the viscous torque which opposes locked mode formation is due to a combination of anomalous perpendicular ion viscosity and neoclassical toroidal flow damping [20–22] induced by the non-axisymmetric harmonics of the error-field. This is appropriate in situations in which the flow damping is sufficiently strong to relax the ion toroidal velocity in the vicinity of the resonant surface to a fixed value determined by neoclassical theory. The scaling of the error-field penetration threshold predicted by the Cole, Hegna and Callen model (in the first semi-collisional layer response regime, and the so-called $1/\nu$ toroidal flow damping regime [22]) takes the form

$$\left(\frac{b_r}{B_T}\right)_{crit} \sim \beta\,\nu_*^{-1/2}\,\rho_*^{3/2} \sim n_e^{1/2}\,T_i^{11/4}\,B_T^{-7/2}\,R_0^{-2} \sim n_e^{1/2}\,B_T^{-13/10}\,R_0^{-5/8}. \quad (4)$$

The predicted scaling with engineering parameters is an improvement on that of the Cole and Fitzpatrick model, since it exhibits a stronger density dependence. Unfortunately, this dependence still appears to be too weak to explain the experimental data.

The model presented in this paper is similar to that of Cole, Hegna and Callen, except that the response of the plasma

in the vicinity of the resonant surface to the applied error-field is calculated from nonlinear drift-MHD island physics [23, 24], rather than linear layer physics. This is appropriate in situations in which, prior to locked mode formation, error-field driven reconnection is not suppressed to such an extent that the nonlinear island width is less than the linear layer width. As we shall see, the scaling of the error-field predicted by this new model (in the so-called polarization regime, and the $1/\nu$ toroidal flow damping regime) is

$$\left(\frac{b_{\rm r}}{B_{\rm T}}\right)_{\rm crit} \sim \beta\,\rho_* \sim n_{\rm e}\,T_{\rm i}^{\,3/2}\,B_{\rm T}^{-3}\,R_0^{-1} \sim n_{\rm e}\,B_{\rm T}^{-9/5}\,R_0^{-1/4}. \quad (5)$$

Thus, the new model captures the linear scaling of the penetration threshold with density that is seen in all experiments. Moreover, the predicted scaling of the threshold with toroidal field-strength (and, hence, with major radius) falls within the experimentally determined range. Using this model to extrapolate from JET, we deduce an error-field penetration threshold in ITER of $(b_{\rm r}/B_{\rm T})_{\rm crit} \sim 5\times10^{-5}$ which (just) lies within the expected capabilities of the ITER error-field correction system.

This paper is organized as follows. Section 2 introduces the nonlinear drift-MHD magnetic island evolution equations used to calculate the response of the plasma in the vicinity of the resonant surface to the applied error-field. Section 3 describes the error-field penetration regimes derived from the aforementioned equations. The scaling of the penetration thresholds associated with the various regimes is investigated in section 4. Finally, the paper is summarized in section 5.

## 2. Preliminary analysis

### 2.1. Fundamental definitions

Consider a large aspect-ratio, low-$\beta$, circular cross-section, tokamak plasma of major radius $R_0$, and toroidal magnetic field-strength $B_{\rm T}$. We adopt a conventional, right-handed, quasi-cylindrical, toroidal coordinate system, $(r,\theta,\varphi)$, whose symmetry axis ($r=0$) coincides with the magnetic axis of the plasma. The coordinate $r$ also serves as a label for the equilibrium magnetic flux-surfaces. Let the equilibrium toroidal magnetic field and toroidal plasma current both run in the $+\varphi$ direction. Suppose that a helical magnetic island chain, with $m_\theta$ poloidal periods, and $n_\varphi$ toroidal periods, is embedded within the aforementioned plasma. The island chain is assumed to be radially localized in the vicinity of its associated resonant surface, minor radius $r_{\rm s}$, which is defined as the equilibrium magnetic flux-surface where $q(r_{\rm s}) = m_\theta/n_\varphi \equiv q_{\rm s}$. Here, $q(r)$ is the safety-factor profile. Let the full radial width of the island chain's magnetic separatrix be $4w$. In the following, it is assumed that $\epsilon_{\rm s} \equiv r_{\rm s}/R_0 \ll 1$ and $w/r_{\rm s} \ll 1$.

It is helpful to define the magnetic shear length, $L_{\rm s} \equiv R_0\,q_{\rm s}/({\rm d}\ln q/{\rm d}\ln r)_{r_{\rm s}}$, and the density scale length, $L_n \equiv -r_{\rm s}/({\rm d}\ln n/{\rm d}\ln r)_{r_{\rm s}}$. Here, $n(r)$ is the electron number density profile. (It is assumed that $L_{\rm s}$, $L_n > 0$.) It is also helpful to define the ion diamagnetic frequency, $\omega_{*\,{\rm i}} \equiv k_\theta\,T_{\rm i}/(e\,B_{\rm T}\,L_n)$, the ion beta, $\beta \equiv \mu_0\,n_{\rm e}\,T_{\rm i}/B_{\rm T}^2$, the ion gyroradius, $\rho_{\rm i} \equiv (T_{\rm i}/m_{\rm i})^{1/2}/(e\,B_{\rm T}/m_{\rm i})$, and the ion sound radius, $\rho_{\rm s} \equiv \tau^{\,1/2}\,\rho_{\rm i}$, where $n_{\rm e} \equiv n(r_{\rm s})$, $k_\theta \equiv m_\theta/r_{\rm s}$, $\tau \equiv T_{\rm e}/T_{\rm i}$, $T_{\rm i}$ is the ion temperature, $T_{\rm e}$ is the electron temperature, $e$ is the magnitude of the electron charge (as well as the ion charge) and $m_{\rm i}$ is the ion mass. Both of the aforementioned temperatures are evaluated at the resonant surface.

Let $\nu_{\theta\,{\rm i}}$ be the neoclassical ion poloidal flow damping rate [25], and $\nu_{\varphi\,{\rm i}}$ the neoclassical ion toroidal flow damping rate [22]. Both damping rates are evaluated at the resonant surface, and any radial variation in these rates across the island region is neglected.

The hydromagnetic timescale, the resistive diffusion timescale, the momentum confinement timescale and the particle confinement timescale are defined $\tau_{\rm H} \equiv R_0\,(\mu_0\,m_{\rm i}\,n_{\rm e}/B_{\rm T}^2)^{1/2}$, $\tau_{\rm R} \equiv \mu_0\,r_{\rm s}^2/\eta_\parallel$, $\tau_{\rm M} \equiv n_{\rm e}\,m_{\rm i}\,r_{\rm s}^2/\mu_{\perp i}$, and $\tau_{\rm P} \equiv r_{\rm s}^2/D_\perp$, respectively. Here, $\eta_\parallel$ is the parallel electrical resistivity, $\mu_{\perp i}$ the phenomenological perpendicular ion viscosity (due to small scale plasma turbulence) and $D_\perp$ the phenomenological perpendicular particle diffusivity (likewise, due to small scale plasma turbulence). Again, all transport coefficients are evaluated at the resonant surface, and any radial variation in these coefficients across the island region is neglected.

### 2.2. Island evolution equations

In this paper, it is assumed that the response of the plasma in the vicinity of the resonant surface to the applied error-field is governed by the strong poloidal flow damping regime/low toroidal flow damping limit magnetic island evolution equations derived in [24]. These equations take the form

$$4I_1\,\tau_{\rm R}\,\frac{{\rm d}}{{\rm d}t}\left(\frac{w}{r_{\rm s}}\right) = -2m_\theta + 2m_\theta\left(\frac{w_{\rm v}}{w}\right)^2\cos\phi - I_{\rm p}\,\beta_0\left(\frac{w_0}{r_{\rm s}}\right)^2\frac{r_{\rm s}^3}{w^3+\rho_{\rm s}^3}, \quad (6)$$

$$-2m_\theta\left(\frac{w_{\rm v}}{w_0}\right)^2\left(\frac{w}{r_{\rm s}}\right)^2\sin\phi = 4\,\beta_0\left(\frac{\nu_{\varphi\,{\rm i}}}{\tau_{\rm M}\,\omega_{*\,{\rm i}}^2}\right)^{1/2}\left(\frac{1}{\omega_{*\,{\rm i}}}\frac{{\rm d}\phi}{{\rm d}t} - \nu_{\rm nc} - \nu_{\rm f}\right). \quad (7)$$

Here, for the sake of simplicity, the stability index for the $m_\theta$, $n_\varphi$ tearing mode [26] is given the vacuum value $\Delta'\,r_{\rm s} = -2m_\theta$. Moreover, $4w$ is the full radial width of the true island chain, $4w_{\rm v}$ is the full radial width of the vacuum island chain associated with the resonant harmonic of the error-field and $\phi$ is the helical phase difference between the true island chain and the vacuum island chain. In addition, $I_1 = 0.8227$, and $\nu_{\rm nc} \equiv k_\theta\,V_{\rm p}^{\rm nc}/\omega_{*\,{\rm i}}$, where $V_{\rm p}^{\rm nc}$ is the so-called neoclassical phase velocity: i.e. the phase velocity that the island chain would have were it to simply co-rotate with the equilibrium ion fluid at the resonant surface. As a consequence of the poloidal and toroidal flow damping present in the plasma, the poloidal and toroidal components of the unperturbed (by the island) ion fluid velocity at the resonant surface are both constrained to take fixed values determined by neoclassical theory. It follows

that the neoclassical phase velocity is also fixed by neoclassical theory. Finally,

$$w_0 \equiv \frac{\rho_{\rm i}}{\delta}, \tag{8}$$

$$\beta_0 \equiv \frac{\beta}{\delta^2}, \tag{9}$$

$$\delta \equiv \left(\frac{L_n}{L_{\rm s}}\,\frac{\epsilon_{\rm s}}{q_{\rm s}}\right)^{1/2}. \tag{10}$$

Equation (6) governs the time evolution of the island chain's radial width [27, 28]. The first term on the right-hand side is due to the intrinsic MHD stability of the $m_\theta, n_\varphi$ tearing mode (the fact that this term is negative indicates that the mode is intrinsically stable). The second term specifies the destabilizing effect of the resonant harmonic of the applied error-field. Finally, the third term parametrizes the stabilizing effect (since $I_{\rm p} > 0$—see the appendix) of the ion polarization current induced by the propagation of the island chain relative to the local ion fluid in circumstances in which this fluid cannot easily cross the magnetic separatrix [29, 30].

The ion polarization term in equation (6) has a slightly different form to that specified in [24]: i.e. its denominator is $w^3 + \rho_{\rm s}^3$, rather than $w^3$. This modification has been made to incorporate additional physics into the model. To be more explicit, as discussed in [23], when $w \gg \rho_{\rm s}$ the island chain lies in the so-called sonic regime. In this regime, the ion fluid cannot easily cross the island separatrix, and the polarization term (which is stabilizing) varies with island width as $w^{-3}$. On the other hand, as $w \to \rho_{\rm s}$ the island chain enters the so-called hypersonic regime. In this regime, the ion fluid can pass almost freely through the separatrix, and the polarization term (which is again stabilizing) exhibits no strong variation with island width. The modification to the polarization term in equation (6) is meant to incorporate hypersonic island physics into the plasma response model. According to this modification, the polarization term ceases to increase like $w^{-3}$ as $w \to \rho_{\rm s}$, but instead asymptotes to a fixed value. The basic reason for this behavior is the decoupling of the ion fluid from the island chain as $w \to \rho_{\rm s}$.

Equation (7) specifies how the phase evolution of the island chain is governed by the balance of the electromagnetic locking torque due to the error-field (left-hand side) and the viscous restoring torque (right-hand side) that develops when the chain does not propagate at its natural frequency: i.e. its propagation frequency in the absence of the error-field. The natural frequency is defined $\omega_0 \equiv v_0\,\omega_{*\rm i}$, where $v_0 \equiv v_{\rm f} + v_{\rm nc}$.

If, during the solution of equations (6) and (7), the island width $w$ ever passes through zero and becomes negative then the situation is easily rectified by making the transformation $w \to -w$ and $\phi \to \phi - \pi$. In other words, an island chain of negative width is equivalent to an island chain of positive width with the X- and O-points interchanged.

The neoclassical toroidal flow damping is assumed to lie in the so-called $1/\nu$ regime, in which it is dominated by toroidally trapped ions. Consequently, the toroidal flow damping rate can be written [19, 22] as

$$\nu_{\varphi\,\rm i} = \frac{n_\varphi^2\,\omega_{\rm tr\,i}^2}{\nu_{\rm i}}\,q_{\rm s}^2\,\epsilon_{\rm s}^{3/2}\,\Lambda^2\left(\frac{m_\theta\,w_{\rm v}^2}{r_{\rm s}\,L_{\rm s}}\right)^2. \tag{11}$$

Here, $\omega_{{\rm tr}\,i} \equiv (T_{\rm i}/m_{\rm i})^{1/2}/L_{\rm s}$ is the ion transit frequency, $\nu_{\rm i} \equiv \tau^{3/2}\,(m_{\rm e}/m_{\rm i})^{1/2}\,(n_{\rm e}\,e^2\,\eta_\parallel/m_{\rm e})$ is the ion collision frequency, $m_{\rm e}$ is the electron mass and $\Lambda$ is (to within a constant of order unity) the ratio of $\delta B/B_{\rm T}$ to $b_{\rm r}/B_{\rm T} \equiv (m_\theta\,w_{\rm v}^2/r_{\rm s}\,L_{\rm s})$, where $\delta B$ is the net toroidal modulation of the magnetic field-strength produced by all harmonics of the error-field, and $b_{\rm r}$ is the resonant harmonic of the vacuum radial error-field. Both $\delta B$ and $b_{\rm r}$ are evaluated at the resonant surface.

The strong poloidal flow damping regime ordering used to derive equations (6) and (7) is valid provided

$$(\epsilon_{\rm s}/q_{\rm s})^2\,\nu_{\theta\,\rm i} \gg \omega_{*\rm i} \gg \nu_{\varphi\,\rm i}, \tag{12}$$

and

$$\delta \ll 1. \tag{13}$$

This regime is also consistent with the orderings $(\epsilon_{\rm s}/q_{\rm s}) \sim \delta$, and $\beta \sim \delta^4$. (The ordering $\beta \lesssim \delta^4$ is dictated by the requirement that the ion polarization term in the island width evolution equation not violate the constant-$\psi$ approximation [26].) In addition, the low toroidal flow damping limit ordering employed in the derivation of the island evolution equations is valid as long as

$$\nu_{\varphi\,\rm i}\,\tau_{\rm M} \ll \frac{r_{\rm s}^2}{w^2}. \tag{14}$$

The assumption that the plasma response in the vicinity of the resonant surface is governed by nonlinear magnetic island physics, rather than linear layer physics, is valid provided that the linear layer width is much less than the island width. In the so-called visco-resistive layer regime [12], this requirement reduces to

$$\left(\frac{\tau_{\rm H}}{\tau_{\rm R}}\right)^{1/6}\left(\frac{\tau_{\rm H}}{\tau_{\rm M}}\right)^{1/6} r_{\rm s} \ll w. \tag{15}$$

The parameter $v_{\rm f} \equiv v_0 - v_{\rm nc}$, which specifies the island's unperturbed (by the error-field) phase velocity relative to its neoclassical phase velocity, as well as the parameter $I_{\rm p}$, which multiplies the ion polarization term in equation (6), can be determined by means of the procedure set out in the appendix. Note that $v_{\rm f} > 0$, which indicates that the island chain propagates in the electron diamagnetic direction relative to the local ion fluid. Furthermore, $I_{\rm p} > 0$, which indicates that the ion polarization current generated by the aforementioned propagation is stabilizing.

Finally, any influence of the perturbed bootstrap current [31] and magnetic field-line curvature [32] on the evolution of the island chain has been neglected in equations (6) and (7), since such effects are only important for relatively wide island chains, and are, therefore, not germane to a discussion of error-field penetration.

### 2.3. *Normalized island evolution equations*

Let $T \equiv |\omega_0|\,t$, $\Phi \equiv {\rm sgn}(\omega_0)\,\phi$, $y \equiv (w/w_0)^3$ and $y_v \equiv (w_{\rm v}/w_0)^3$. The island evolution equations (6) and (7) reduce to

$$C_1\,\frac{{\rm d}y}{{\rm d}T} = -y^{2/3} + y_{\rm v}^{2/3}\,\cos\Phi - C_2\,F(y), \tag{16}$$

$$\frac{{\rm d}\Phi}{{\rm d}T} = 1 - C_3\,y^{2/3}\,\sin\Phi, \tag{17}$$

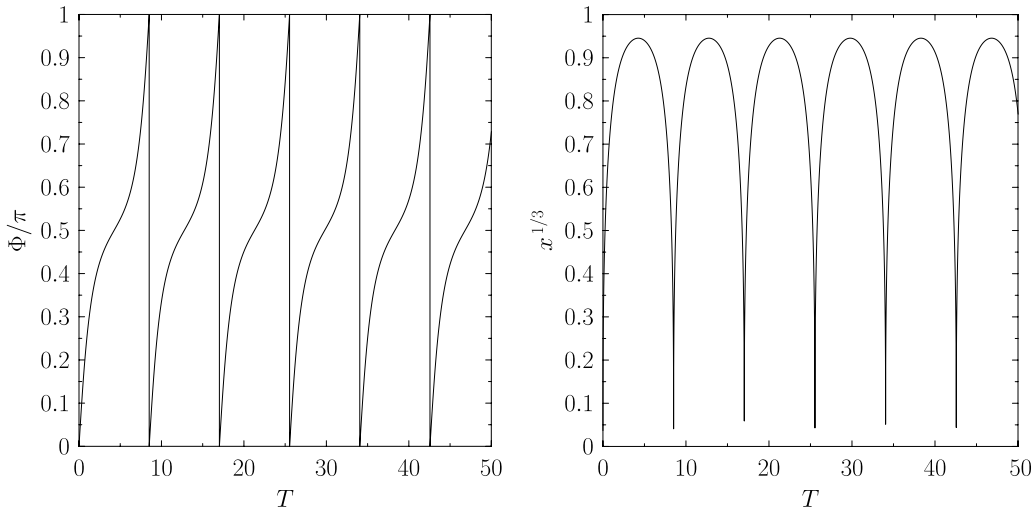


**Figure 1.** A typical rotating solution in the Rutherford error-field penetration regime. The left-hand panel shows the time variation of the relative phase, $\Phi$, between the island chain and the vacuum island chain. The right-hand panel shows the time variation of the normalized island width, $x^{1/3}$. Calculation performed with $\hat{x}_{\rm v} = 0.35$.

where

$$C_1 \equiv \frac{2\,I_1}{3}\,\frac{|v_0|\,\tau_{\rm R}\,\omega_{*\rm i}}{m_\theta}\,\frac{w_0}{r_{\rm s}}, \tag{18}$$

$$C_2 \equiv \frac{I_{\rm p}}{54^{\,1/3}}\,\frac{\beta_0}{m_\theta\,\tau^{\,1/2}}\,\frac{r_{\rm s}}{\rho_{\rm i}}, \tag{19}$$

$$C_3 \equiv \frac{m_\theta}{2\,\beta_0}\,\frac{\tau_{\rm D}^{\,1/2}\,\tau_{\rm M}^{\,1/2}\,\omega_{*\rm i}}{|v_0|}\left(\frac{w_0}{r_{\rm s}}\right)^2, \tag{20}$$

and

$$F(y) \equiv \frac{3}{2^{\,2/3}}\,\frac{\tau^{\,1/2}\,\delta\,y^{\,2/3}}{y+\tau^{\,3/2}\,\delta^{\,3}}, \tag{21}$$

$$\tau_{\rm D} \equiv \left(\frac{w_{\rm v}}{w_0}\right)^4 \nu_{\varphi\,\rm i}^{-1} = \frac{\nu_{\rm i}}{n_\varphi^{\,2}\,\omega_{\rm tr\,i}^{\,2}}\,\frac{1}{q_{\rm s}^{\,2}\,\epsilon_{\rm s}^{\,3/2}\,\Lambda^{\,2}}\left(\frac{r_{\rm s}\,L_{\rm s}}{m_\theta\,w_0^{\,2}}\right)^2. \tag{22}$$

Here, $\tau_{\rm D}$ is termed the toroidal flow damping timescale. Observe that $0 \leqslant F(y) \leqslant 1$.

Let $x \equiv C_3^{\,3/2}\,y$ and $x_v \equiv C_3^{\,3/2}\,y_v$. The normalized layer equations (16) and (17) transform to

$$D_1\,\frac{{\rm d}x}{{\rm d}T} = -x^{\,2/3} + x_{\rm v}^{\,2/3}\,\cos\Phi - D_2\,G(x), \tag{23}$$

$$\frac{d\Phi}{{\rm d}T} = 1 - x^{\,2/3}\,\sin\Phi, \tag{24}$$

where

$$D_1 \equiv \frac{C_1}{C_3^{\,1/2}}, \tag{25}$$

$$D_2 \equiv C_2\,C_3, \tag{26}$$

$$G(x) \equiv \frac{3}{2^{\,2/3}}\,\frac{d\,x^{\,2/3}}{x+d^{\,3}}, \tag{27}$$

$$d \equiv \tau^{\,1/2}\,C_3^{\,1/2}\,\delta. \tag{28}$$

Observe that $0 \leqslant G(x) \leqslant 1$. The parameters $D_1$ and $D_2$ measure the degree of shielding (prior to penetration) of the resonant harmonic of the error-field by the plasma in the vicinity of the resonant surface that is due to neoclassical flow and the ion polarization current, respectively.

## 3. Nonlinear error-field penetration regimes

### *3.1. Rutherford regime*

In the so-called Rutherford error-field penetration regime (which is named after a somewhat similar regime described in [12]), the first and the third terms on the right-hand side of the island width evolution equation, (23), are assumed to be negligible. Defining $\hat{x}_{\rm v} \equiv x_v/D_1^{\,3/2}$, where it is assumed that $\hat{x}_{\rm v} \sim 1$ (because we shall presently show that (29) and (30) can only be solved when $0 \leqslant \hat{x}_{\rm v} < 0.3685$), equations (23) and (24) reduce to

$$\frac{{\rm d}x}{{\rm d}T} \simeq \hat{x}_{\rm v}^{\,2/3}\,\cos\Phi, \tag{29}$$

$$\frac{{\rm d}\Phi}{{\rm d}T} = 1 - x^{\,2/3}\,\sin\Phi. \tag{30}$$

The approximations used to derive the above pair of equations are valid provided

$$D_1 \gg 1,\ D_2: \tag{31}$$

i.e. as long as shielding due to neoclassical flow is strong, and also dominates shielding due to the ion polarization current. As discussed below, equations (29) and (30) possess two different types of solution, depending on the value of the parameter $\hat{x}_{\rm v}$.

For $0 \leqslant \hat{x}_{\rm v} < 0.3685$, the relative phase, $\Phi$, between the island chain and the vacuum island chain increases continually in time: i.e. the island chain rotates with respect to the vacuum chain. A typical rotating solution is shown in figure 1. Note that the island width "pulsates" on a normalized timescale $T \sim 1$, and periodically falls to zero when $\Phi = \pi$. Moreover, each time the island width becomes zero, the relative phase between the island chain and the vacuum chain changes abruptly from $\pi$ to 0. As a consequence of these abrupt changes, the relative phase is constrained to lie in the range $0 \leqslant \Phi \leqslant \pi$. However, $\Phi$ spends as much time in the subrange $0 \leqslant \Phi \leqslant \pi/2$, as in the subrange $\pi/2 < \Phi \leqslant \pi$, implying that the error-field has a destabilizing influence on the island chain half of the time,

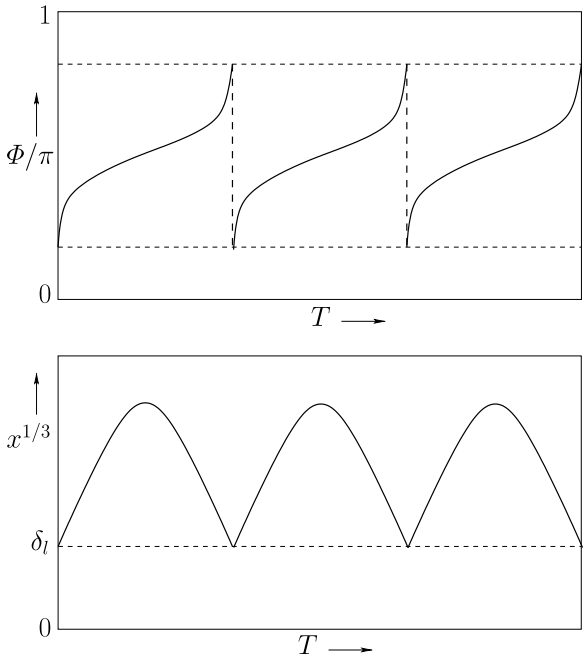


**Figure 2.** Schematic diagram indicating how the behavior shown in figure 1 is modified when the normalized linear layer width, $\delta_l$, becomes comparable with the similarly normalized pulsating island width, $x^{1/3}$.

and a stabilizing influence the other half. This explains why the island width pulsates, rather than growing continually. The mean island width associated with a rotating solution is such that $w \sim D_1^{-1/2}\, w_{\rm v} \ll w_{\rm v}$. In other words, the mean island width is much less than the vacuum island width, indicating strong shielding of the resonant harmonic of the error-field by the plasma in the vicinity of the resonant surface.

Figure 2 shows, schematically, how the behavior described above is modified when the linear layer width becomes comparable with the pulsating island width. As is well known, plasma is trapped inside the magnetic separatrix of a nonlinear magnetic island chain, giving rise to a no slip constraint, according to which changes in the local perpendicular plasma flow must be mirrored by changes in the island phase velocity [11]. However, the no slip constraint is relaxed as soon as the island width falls below the linear layer width. In other words, the island chain is no longer dragged along by the local plasma flow, and is free to adopt any phase relation with respect to the error-field. Thus, in figure 2, as soon as the island chain is dragged sufficiently out of phase with the error-field that its width is reduced to the linear layer width, its phase adjusts itself such as to enable renewed island growth. Moreover, as the linear layer width increases, relative to the island width, the pulsations in the island width, and the oscillations in the island phase, gradually decrease in amplitude, until the island width and phase both become constant in time (with the island width less than the linear layer width). Of course, this is the scenario envisaged in linear error-field penetration theory [11].

For $\hat{x}_{\rm v} \geqslant 0.3685$, the island chain eventually locks to the vacuum island chain in such a manner that its relative phase, $\Phi$, asymptotes to a constant value. Furthermore, this value is always such that the error-field destabilizes the island chain (i.e. $-\pi/2 < \Phi < \pi/2$). A typical locked solution is shown in figure 3. Unlike the rotating solution, the island width increases continually in time. In order to find the final saturated island width, we must employ a second normalization scheme. Defining $\hat{x}_{\rm v} \equiv x_{\rm v}/D_1^{3/2}$, $\hat{x} \equiv x/D_1^{3/2}$, $\hat{T} \equiv T/D_1^{3/2}$ and $\hat{\Phi} \equiv D_1\,\Phi$, and assuming that $\hat{x}_{\rm v}, \hat{x}, \hat{T}, \hat{\Phi} \sim 1$, equations (23) and (24) reduce to

$$\frac{{\rm d}\hat{x}}{{\rm d}\hat{T}} \simeq -\hat{x}^{\,2/3} + \hat{x}_{\rm v}^{\,2/3}, \tag{32}$$

$$0 \simeq 1 - \hat{x}^{\,2/3}\,\hat{\Phi}. \tag{33}$$

This ordering is designed to retain all terms in (29) and (30) except the ${\rm d}\Phi/{\rm d}T$ term, which becomes negligible once the island chain locks, whilst allowing for saturation (which involves introducing the $\hat{x}^{\,2/3}$ term into (32)), and, finally, ensuring that all terms in (32) and (33) are of similar magnitude. The above equations, which are valid as long as inequality (31) is satisfied, imply that the island width and relative phase asymptote to $w = w_{\rm v}$ (which is equivalent to $\hat{x} = \hat{x}_{\rm v}$) and $\Phi \sim D_1^{-1} \ll 1$, respectively, on a normalized timescale $T \sim D_1^{3/2} \gg 1$. Thus, the island chain eventually locks in phase with, and grows to the same width as, the vacuum island chain. This state of affairs is termed full reconnection, since it implies zero shielding of the resonant harmonic of the error-field by the plasma in the vicinity of the resonant surface.

In summary, the Rutherford error-field penetration regime is characterized by strong shielding of the resonant harmonic of the error-field, followed by full reconnection once the penetration threshold has been exceeded. The shielding is a consequence of neoclassical flow at the resonant surface. The critical vacuum island width above which penetration occurs is

$$\left(\frac{w_{\rm v}}{w_0}\right)_{\rm crit} = (y_v)_{\rm crit}^{1/3} = \frac{(x_v)_{\rm crit}^{1/3}}{C_3^{1/2}}$$
$$= c^{\,1/3}\left(\frac{D_1}{C_3}\right)^{1/2} = c^{\,1/3}\,C_1^{1/2}\,C_3^{-3/4}, \tag{34}$$

where $c = 0.3685$, and use has been made of (25).

### 3.2. *Polarization regime*

In the so-called polarization error-field penetration regime, the term on the left-hand side, and the first term on the right-hand side, of the island width evolution equation, (23), are assumed to be negligible. Defining $\hat{x}_{\rm v} \equiv x_{\rm v}/D_2^{3/2}$ and $\hat{x} \equiv x/d^{\,3}$, and assuming that $\hat{x}_{\rm v}, \hat{x} \sim 1$ (because we shall presently show that (35) and (36) can only be solved when $0 \leqslant \hat{x}_{\rm v} \leqslant 1$ and $0 \leqslant \hat{x} \leqslant 2$), equations (23) and (24) reduce to

$$0 \simeq \hat{x}_{\rm v}^{\,2/3}\,\cos\Phi - H(\hat{x}), \tag{35}$$

$$\frac{{\rm d}\Phi}{{\rm d}T} = 1 - d^{\,2}\,\hat{x}^{\,2/3}\,\sin\Phi, \tag{36}$$

where

$$H(\hat{x}) \equiv \frac{3}{2^{\,2/3}}\,\frac{\hat{x}^{\,2/3}}{\hat{x}+1}. \tag{37}$$

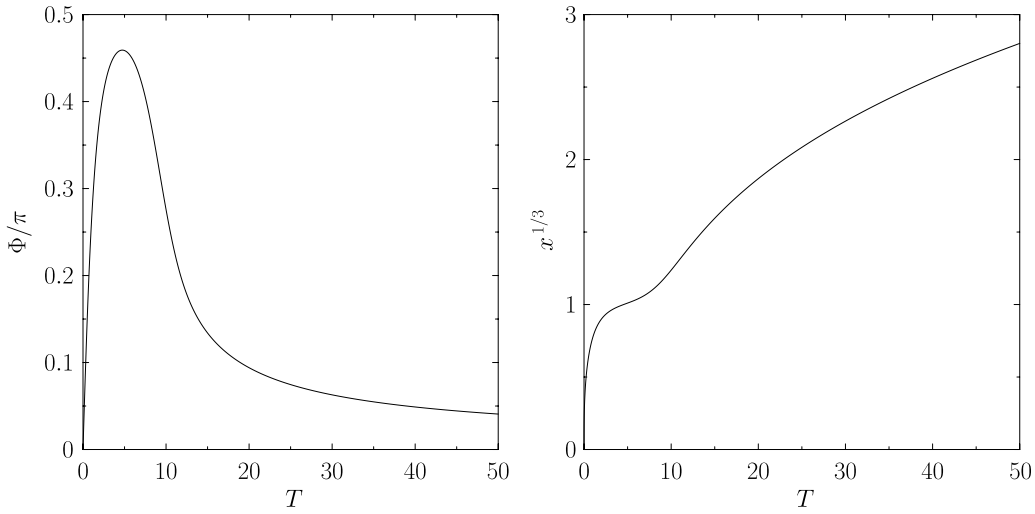


**Figure 3.** A typical locked solution in the Rutherford error-field penetration regime. The left-hand panel shows the time variation of the relative phase, $\Phi$, between the island chain and the vacuum island chain. The right-hand panel shows the time variation of the normalized island width, $x^{1/3}$. Calculation performed with $\hat{x}_{\rm v} = 0.38$.

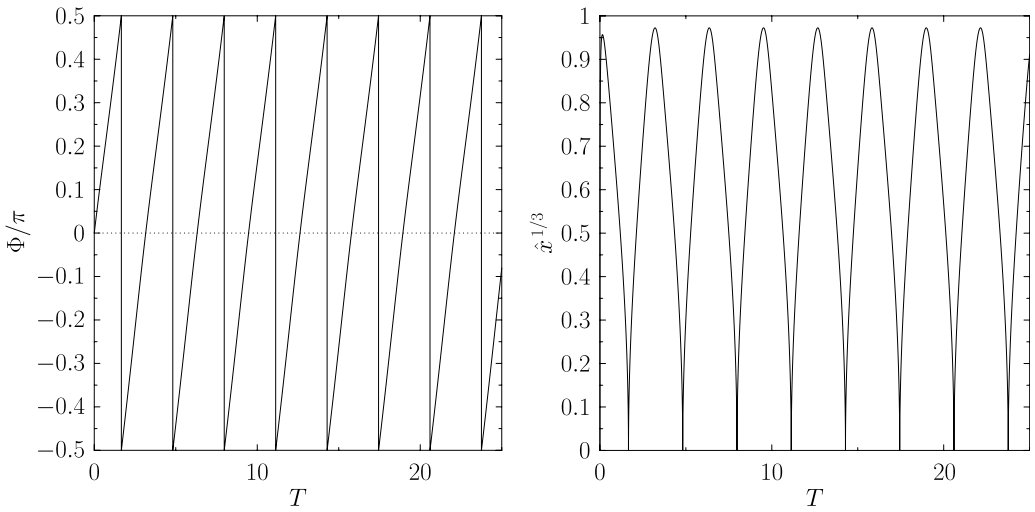


**Figure 4.** A typical rotating solution in the polarization error-field penetration regime. The left-hand panel shows the time variation of the relative phase, $\Phi$, between the island chain and the vacuum island chain. The right-hand panel shows the time variation of the normalized island width, $\hat{x}^{1/3}$. Calculation performed with $\hat{x}_{\rm v} = 0.9$ and $d = 0.5$.

Observe that $0 \leqslant H(\hat{x}) \leqslant 1$, and that $H(\hat{x})$ attains its peak value of unity at $\hat{x} = 2$. The approximations used to derive equations (35) and (36) are valid provided

$$D_2 \gg d^{\,2},\, D_1\, d^{\,3}\,: \tag{38}$$

i.e. provided that shielding due to the ion polarization current is strong, and also dominates shielding due to neoclassical flow.

We suppose, for the sake of argument, that

$$d < 2^{\,-1/3}. \tag{39}$$

In this case, since $0 \leqslant H(\hat{x}) \leqslant 1$, it is possible to find rotating solutions of (35) and (36), in which the relative phase between the island chain and the vacuum island chain increases continually in time, when $0 \leqslant \hat{x}_{\rm v} \leqslant 1$. Such solutions are characterized by $\hat{x} < 2$ and $d^{\,2}\,\hat{x}^{\,2/3} < 1$. A typical rotating solution is shown in figure 4. As before, the island width pulsates on a normalized timescale $T \sim 1$, periodically falling to zero when $\Phi = \pi/2$. Each time the island width becomes zero, the relative phase changes abruptly from $\pi/2$ to $-\pi/2$. As a consequence of these abrupt changes, the relative phase is constrained to lie in the range $-\pi/2 \leqslant \Phi \leqslant \pi/2$. Thus, the island chain is always destabilized by the error-field. The island width is, however, prevented from increasing by the strong stabilizing influence of the ion polarization current. The mean island width of a rotating solution is such that $w \sim D_2^{-1/2}\, d\, w_{\rm v} \ll w_{\rm v}$. In other words, the mean island width is much less than the vacuum island width, indicating strong shielding of the resonant harmonic of the error-field by the plasma in the vicinity of the resonant surface.

When $\hat{x}_{\rm v} > 1$, the rotating solution of equations (35) and (36) breaks down close to $\Phi = 0$, indicating that we need to look for another type of solution. Defining $\hat{x}_{\rm v} \equiv x_{\rm v}/D_2^{\,3/2}$, $\hat{x} \equiv x/(D_2/D_1)^{\,3/5}$, $\hat{T} \equiv T/(D_1/D_2)^{\,2/5}$, and $\hat{\Phi} \equiv \Phi/(D_1/D_2)^{\,2/5}$, and assuming that $\hat{x}_{\rm v}$, $\hat{x}$, $\hat{T}$ and $\hat{\Phi} \sim 1$,

equations (23) and (24) reduce to

$$\frac{\mathrm{d}\hat{x}}{\mathrm{d}\hat{T}} \simeq \hat{x}_{\mathrm{v}}^{\,2/3}, \tag{40}$$

$$\frac{\mathrm{d}\hat{\Phi}}{\mathrm{d}\hat{T}} \simeq 1 - \hat{x}^{\,2/3}\,\hat{\Phi}. \tag{41}$$

This ordering is designed to retain all terms in (35) and (36) except the polarization term, which becomes negligible once the island width increases to such an extent that $x \gg d^{\,3}$, whilst allowing for island growth (which involves introducing the $\mathrm{d}\hat{x}/\mathrm{d}\hat{T}$ term into (40)), and, finally, ensuring that all terms in (40) and (41) are of similar magnitude. The above equations are valid provided the inequalities

$$D_2 \gg D_1, \tag{42}$$

$$D_1^{\,2/3}\,D_2 \gg 1 \tag{43}$$

are both satisfied. According to equations (40) and (41), the island width grows linearly in time, while the relative phase between the island chain and the vacuum chain grows as $T$ when $T \ll (D_1/D_2)^{2/5}$, attains a maximum value $\Phi \sim (D_1/D_2)^{2/5} \ll 1$ when $T \sim (D_1/D_2)^{2/5}$, and then decays as $T^{\,-2/3}$ when $T \gg (D_1/D_2)^{2/5}$. In other words, the island chain locks in phase with the vacuum chain on a normalized timescale $T \sim (D_1/D_2)^{2/5} \ll 1$.

In order to determine the saturated island width, we must adopt a third ordering scheme. Defining $\hat{x}_{\mathrm{v}} \equiv x_{\mathrm{v}}/D_2^{\,3/2}$, $\hat{x} \equiv x/D_2^{\,3/2}$, $\hat{T} \equiv T/(D_1\,D_2^{\,1/2})$ and $\hat{\Phi} \equiv D_2\,\Phi$, and assuming that $\hat{x}_{\mathrm{v}}, \hat{x}, \hat{T}, \hat{\Phi} \sim 1$, equations (23) and (24) reduce to

$$\frac{\mathrm{d}\hat{x}}{\mathrm{d}\hat{T}} \simeq -\hat{x}^{\,2/3} + \hat{x}_{\mathrm{v}}^{\,2/3}, \tag{44}$$

$$0 \simeq 1 - \hat{x}^{\,2/3}\,\hat{\Phi}. \tag{45}$$

This ordering is designed to retain all terms in (40) and (41) except the $d\hat{\Phi}/\mathrm{d}\hat{T}$ term, which becomes negligible once the island chain locks, whilst allowing for island saturation (which involves introducing the $\hat{x}^{\,2/3}$ term into (44)), and, finally, ensuring that all terms in (44) and (45) are of similar magnitude. The above equations, which are valid as long as the inequalities (39), (42) and (43) are satisfied, imply that the island width and the relative phase asymptote to $w = w_{\mathrm{v}}$ (which is equivalent to $\hat{x} = \hat{x}_{\mathrm{v}}$) and $\Phi \sim D_2^{\,-1} \ll (D_1/D_2)^{2/5}$, respectively, on a normalized timescale $T \sim D_1\,D_2^{\,1/2} \gg (D_1/D_2)^{2/5}$. In other words, the island chain eventually achieves full reconnection.

In summary, the polarization error-field penetration regime is characterized by strong shielding of the resonant harmonic of the error-field, followed by full reconnection once the penetration threshold has been exceeded. The shielding is a consequence of the ion polarization current. The critical vacuum island width above which penetration occurs is

$$\left(\frac{w_{\mathrm{v}}}{w_0}\right)_{\mathrm{crit}} = (y_{\mathrm{v}})_{\mathrm{crit}}^{\,1/3} = \frac{(x_{\mathrm{v}})_{\mathrm{crit}}^{\,1/3}}{C_3^{\,1/2}} = \left(\frac{D_2}{C_3}\right)^{1/2} = C_2^{\,1/2}, \tag{46}$$

where use has been made of (26).

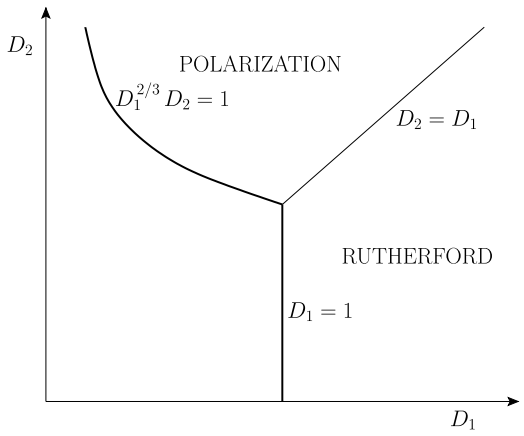


**Figure 5.** Boundaries of the Rutherford and polarization error-field penetration regimes plotted in $D_1$-$D_2$ space.

### *3.3. Summary*

Figure 5 shows the boundaries of the Rutherford and polarization error-field penetration regimes plotted in $D_1$-$D_2$ space. In both regimes, the resonant harmonic of the error-field is strongly shielded by the plasma in the vicinity of the resonant surface until the resonant harmonic exceeds a certain critical magnitude. However, as soon as this occurs, the island chain locks to the vacuum island chain, and the island chain's width subsequently grows until it matches that of the vacuum chain. In the Rutherford regime, penetration is triggered when the electromagnetic locking torque due to the resonant harmonic of the error-field overcomes the viscous torque due to the rotating plasma. On the other hand, in the polarization regime, penetration is triggered when the destabilizing influence of the error-field overcomes the stabilizing influence of the ion polarization current (induced by the rotation of the island chain in the local ion fluid frame—see the appendix). In the region of figure 5 not occupied by the Rutherford and polarization regimes neither neoclassical flow nor the ion polarization current are large enough to cause strong shielding of the resonant harmonic of the error-field by the plasma in the vicinity of the resonant surface. In this situation, error-field driven reconnection always proceeds to full reconnection: i.e. the error-field penetration threshold is effectively zero.

The relationship between the resonant harmonic of the vacuum radial error-field, $b_{\mathrm{r}}$, and the vacuum island width, $w_{\mathrm{v}}$, is

$$\frac{b_{\mathrm{r}}}{B_{\mathrm{T}}} = \frac{m_\theta\,w_{\mathrm{v}}^{\,2}}{r_{\mathrm{s}}\,L_{\mathrm{s}}}, \tag{47}$$

where $b_{\mathrm{r}}$ is evaluated at the resonant surface. Hence, from (34) and (46), the critical value of $b_{\mathrm{r}}$ required to trigger penetration is

$$\left(\frac{b_{\mathrm{r}}}{B_{\mathrm{T}}}\right)_{\mathrm{crit}} = \frac{c^{\,2/3}\,2^{\,5/2}\,I_1}{3}\,\frac{\beta^{\,3/2}\,|v_0|^{\,5/2}}{m_\theta^{\,3/2}\,\delta^{\,3}}\,\frac{\tau_{\mathrm{R}}\,\omega_{*\mathrm{i}}}{(\tau_{\mathrm{D}}^{\,1/2}\,\tau_{\mathrm{M}}^{\,1/2}\,\omega_{*\mathrm{i}})^{\,3/2}}\,\frac{r_{\mathrm{s}}}{L_{\mathrm{s}}} \tag{48}$$

in the Rutherford regime, and

$$\left(\frac{b_{\mathrm{r}}}{B_{\mathrm{T}}}\right)_{\mathrm{crit}} = \frac{I_{\mathrm{p}}}{54^{\,1/3}}\,\frac{\beta}{\delta^{\,4}\,\tau^{\,1/2}}\,\frac{\rho_{\mathrm{i}}}{L_{\mathrm{s}}} \tag{49}$$

in the polarization regime, where use has been made of (18)–(20).

## 4. Scaling of error-field penetration threshold

### 4.1. Preliminary analysis

The standard dimensionless scaling parameters $\beta$, $\nu_*$ and $\rho_*$ [13] are defined:

$$\beta \equiv \frac{\mu_0\, n_e\, T_i}{B_T^2}, \tag{50}$$

$$\nu_* \equiv \frac{L_s\, n_e\, e^2\, \eta_\parallel}{m_e^{1/2}\, T_e^{1/2}}, \tag{51}$$

$$\rho_* \equiv \frac{T_i^{1/2}\, m_i^{1/2}}{e\, B_T\, L_s}. \tag{52}$$

It follows from the definitions in section 2.1, as well as equation (22), that

$$\omega_{*i}\, \tau_H \sim n_\varphi\, \frac{\beta^{1/2}\, \rho_*}{\delta^2}, \tag{53}$$

$$\frac{\tau_R}{\tau_H} \sim \frac{q_s}{\tau^{1/2}} \left(\frac{m_i}{m_e}\right)^{1/2} \left(\frac{\epsilon_s}{q_s}\right)^2 \frac{\beta^{1/2}}{\nu_*\, \rho_*^2}, \tag{54}$$

$$\frac{\tau_D}{\tau_H} \sim \frac{\epsilon_s^{1/2}\, \tau^2}{n_\varphi^4\, q_s^5}\, \frac{\delta^4}{\Lambda^2}\, \frac{\nu_*}{\beta^{1/2}\, \rho_*^4}, \tag{55}$$

where we have neglected any numerical constants of order unity, and have assumed that $L_s \sim q_s\, R_0$. Now, in an ohmically heated tokamak plasma, the energy confinement timescale, $\tau_E$, satisfies the constraint

$$\frac{n_e\, T_i}{\tau_E} \sim \eta_\parallel \left(\frac{B_T}{\mu_0\, L_s}\right)^2, \tag{56}$$

which is obtained by equating the energy loss rate to the ohmic heating rate. We assume that the momentum confinement timescale is similar to the energy confinement timescale, as is generally observed to be the case in ohmically heated tokamak plasmas [33]. It follows that

$$\frac{\tau_M}{\tau_H} \sim \frac{q_s}{\tau^{1/2}} \left(\frac{m_i}{m_e}\right)^{1/2} \frac{\beta^{3/2}}{\nu_*\, \rho_*^2}. \tag{57}$$

Making use of equations (53)–(55) and (57), the three most important parameters defined in section 2.3 take the values

$$d \sim \frac{\epsilon_s^{1/8}\, \tau^{7/8}}{q_s^{1/2}\, |v_0|^{1/2}} \left(\frac{m_i}{m_e}\right)^{1/8} \frac{q_s}{\epsilon_s}\, \frac{\delta}{\Lambda^{1/2}}, \tag{58}$$

$$D_1 \sim |v_0| \left(\frac{m_i}{m_e}\right)^{1/2} \frac{\epsilon_s}{q_s}\, \frac{\beta}{\nu_*\, \delta^2\, d}, \tag{59}$$

$$D_2 \sim \frac{1}{n_\varphi\, q_s\, \tau^{3/2}}\, \frac{\epsilon_s}{q_s}\, \frac{\beta\, d^2}{\rho_*\, \delta^4}. \tag{60}$$

Finally, it follows from equations (48) and (49) that the error-field penetration thresholds in the Rutherford and polarization regimes can be written as

$$\left(\frac{b_r}{B_T}\right)_{crit} \sim n_\varphi\, q_s\, \tau\, |v_0| \left(\frac{m_i}{m_e}\right)^{1/2} \frac{\beta\, \rho_*^2}{\nu_*\, \delta^2\, d^3} \tag{61}$$

and

$$\left(\frac{b_r}{B_T}\right)_{crit} \sim \frac{1}{\tau^{1/2}}\, \frac{\beta\, \rho_*}{\delta^4}, \tag{62}$$

respectively.

### 4.2. Self-consistency check

Our derivation of the polarization error-field penetration threshold, (62), depends on a great many ordering assumptions. We check that—in theory, at least—it is possible to simultaneously satisfy all of these constraints.

Suppose, as seems reasonable in a study of conventional error-field penetration in low density, ohmically heated, tokamak plasmas, that $n_\varphi$, $q_s$, $\tau$, $\epsilon_s^{1/2} \sim 1$. Suppose, further, that $\beta \sim \delta^4$, and $\epsilon_s/q_s \sim \delta$, since these orderings are implicit in the derivation of the island evolution equations introduced in section 2.2. Finally, suppose that $d \sim 1$, which corresponds to choosing the strongest toroidal flow damping rate that is consistent with the analysis of section 3.2. It follows from (58)–(60) that

$$D_1 \sim \frac{|v_0|\, \delta}{\bar\nu}, \tag{63}$$

$$D_2 \sim \frac{\delta}{\rho_*}, \tag{64}$$

where $\bar\nu \equiv (m_e/m_i)^{1/2}\, \nu_*/\delta^2$. Now, if $1 \ll D_1 \ll D_2$, which corresponds to

$$\frac{\bar\nu}{\delta} \ll |v_0| \ll \frac{\bar\nu}{\rho_*}, \tag{65}$$

then the operating point in figure 5 lies in the polarization regime. Furthermore, in this regime, inequalities (12), (14) and (15), which must all be satisfied in order for the island evolution equations used in our analysis to be valid, yield the constraints

$$\frac{\delta^2}{|v_0|^2} \ll \frac{\bar\nu}{\rho_*} \ll 1. \tag{66}$$

Assuming that $|v_0| \gg \delta^{3/2}, \bar\nu/\delta$, the previous two inequalities can be combined to give

$$|v_0| \ll \frac{\bar\nu}{\rho_*} \ll 1. \tag{67}$$

The lower limit on $\bar\nu/\rho_*$ comes from the inequality $D_2 \gg D_1$, whereas the upper limit comes from inequality (15). Inequality (67) implies that expression (62) for the error-field penetration threshold is valid as long as the plasma in the vicinity of the resonant surface is not too collisional, and the natural frequency of the resonant magnetic island chain is small compared with the local ion diamagnetic frequency. Note, incidentally, that the latter restriction is lifted when $d \gtrsim 1$. If $\bar\nu/\rho_* > 1$ then the response of the plasma in the vicinity of the resonant surface to the error-field is governed by linear layer

physics, rather than nonlinear island physics [12]. On the other hand, if $\bar{\nu}/\rho_* < |v_0|$ then the operating point in figure 5 lies in the Rutherford regime, instead of the polarization regime, and expression (62) must be replaced by expression (61). This suggests that the polarization regime is favoured over the Rutherford regime in plasmas with relatively high (but not too high) collisionality and weak flow—i.e. ohmically heated plasmas.

### *4.3. Scaling analysis*

Assuming that inequality (67) is satisfied, which—in theory, at least—is possible, we examine the scaling of the error-field penetration threshold, (62).

Consider, first of all, the scaling with the standard dimensionless parameters $\beta$, $\nu_*$ and $\rho_*$. In fact, it is immediately clear from equation (62) that

$$\left(\frac{b_r}{B_T}\right)_{crit} \sim \beta\,\rho_*. \tag{68}$$

Next, consider the scaling with the physics parameters $n_e$, $T_i$, $B_T$ and $R_0$. Now, according to equations (50)–(52), $\beta \sim n_e\,T_i\,B_T^{-2}$, $\nu_* \sim n_e\,T_i^{-2}\,R_0$ (since $\eta_\parallel \sim T_i^{-3/2}$), and $\rho_* \sim T_i^{1/2}\,B_T^{-1}\,R_0^{-1}$. Hence, we obtain

$$\left(\frac{b_r}{B_T}\right)_{crit} \sim n_e\,T_i^{3/2}\,B_T^{-3}\,R_0^{-1}. \tag{69}$$

Finally, consider the scaling with the engineering parameters $n_e$, $B_T$ and $R_0$. In order to obtain such a scaling, we need to adopt a particular scaling law for the energy confinement timescale, $\tau_E$ (and, hence, for the momentum confinement time, $\tau_M$). Now, the only widely accepted empirical scaling for the energy confinement timescale in low density, ohmically heated, tokamak plasmas is the well-known neo-ALCATOR scaling law [34], according to which [16, 17]

$$B_T\,\tau_E \sim n_e\,B_T\,R_0^3 \tag{70}$$

at fixed $q_{95}$ and aspect-ratio. Unfortunately, the right-hand side of this expression cannot be expressed solely in terms of $\beta$, $\nu_*$ and $\rho_*$. However, if we slightly change the exponent of $R_0$ from 3 to 3.25 then we can write

$$B_T\,\tau_E \sim n_e\,B_T\,R_0^{13/4} \sim \frac{\beta^{5/4}}{\nu_*^{1/4}\,\rho_*^{7/2}}. \tag{71}$$

Now, the ohmic power balance relation (56) yields

$$B_T\,\tau_E \sim \frac{\beta^2}{\nu_*\,\rho_*^3}. \tag{72}$$

Combining the previous two expressions, we obtain

$$\nu_* \sim \beta\,\rho_*^{2/3}, \tag{73}$$

implying that

$$T_i \sim B_T^{4/5}\,R_0^{1/2}, \tag{74}$$

which is very similar to the temperature scaling predicted by the standard neo-ALCATOR energy confinement law: i.e. $T_i \sim B_T^{4/5}\,R_0^{2/5}$. Eliminating $T_i$ between expressions (69) and (74), we finally arrive at

$$\left(\frac{b_r}{B_T}\right)_{crit} \sim n_e\,B_T^{-9/5}\,R_0^{-1/4}. \tag{75}$$

Note that this scaling of the error-field penetration threshold reproduces the linear variation with plasma density that has been observed in all experimental investigations of error-field penetration in low density, ohmically heated, tokamak plasmas [2–8]. Moreover, the predicted variation of the threshold with toroidal magnetic field-strength is intermediate between the $B_T^{-2.9}$ variation found on the COMPASS-D [5] tokamak, and the $B_T^{-1.2}$, $B_T^{-1.0}$ and $B_T^{-0.6}$ variations found on the JET [5], DIII-D [5] and ALCATOR C-MOD [7] tokamaks, respectively. Finally, the predicted variation of the threshold with major radius is consistent with the conventional constraint that $(b_r/B_T)_{crit}$ should be solely a function of the standard dimensionless parameters $\beta$, $\nu_*$ and $\rho_*$ [5, 13].

By contrast, if we perform an analogous scaling study for the predicted error-field penetration threshold in the Rutherford regime, (61), we find that

$$\left(\frac{b_r}{B_T}\right)_{crit} \sim \beta\,\nu_*^{-1}\,\rho_*^2 \sim T_i^4\,B_T^{-4}\,R_0^{-3} \sim B_T^{-4/5}\,R_0^{-1}. \tag{76}$$

As before, the first, second, and third terms on the right-hand side are the scalings with dimensionless parameters, physics parameters, and engineering parameters, respectively. Note that the scaling with engineering parameters exhibits no dependence on the plasma density. Indeed, as is apparent from an examination of expression (2), this particular scaling with engineering parameters is almost indistinguishable from that derived from the original Fitzpatrick (1993) model [11, 12]. Hence, we conclude that, unlike the threshold derived from the polarization regime, the nonlinear error-field penetration threshold derived from the Rutherford regime cannot account for the experimental observations.

An experimental scaling law of the form $(b_r/B_T)_{crit} \sim n_e^{\alpha_n}\,B_T^{\alpha_B}\,R_0^{\alpha_R}$ (with $\alpha_R = 2\,\alpha_n + (5/4)\,\alpha_B$) corresponds to a theoretical scaling law of the form $(b_r/B_T)_{crit} \sim \beta^{\alpha_\beta}\,\nu_*^{\alpha_\nu}\,\rho_*^{\alpha_\rho}$, where $\alpha_\beta = \alpha_n - x$, $\alpha_\nu = x$ and $\alpha_\rho = -(5/3)\,\alpha_B - 2\,\alpha_n - (2/3)\,x$. Here, $x$ is arbitrary. Thus, an experimental scaling law cannot be uniquely mapped to a theoretical scaling law, although the inverse mapping is unique. The former mapping is not unique because in an ohmically heated tokamak plasma (at fixed edge-$q$ and shape) there are only two independent experimental variables—i.e. $n_e$ and $B_T$—whereas there are three independent indices in the theoretical scaling law. It follows that it is impossible to infer a unique theoretical scaling law (for the error-field penetration threshold in ohmically heated tokamak plasmas) from experimental data without the aid of a theoretical model.

## 5. Summary and discussion

A theory has been developed in order to predict the error-field penetration threshold in low density, ohmically heated, tokamak plasmas. The novel feature of this theory is that

the response of the plasma in the vicinity of the resonant surface to the applied error-field is calculated from nonlinear drift-MHD magnetic island theory, rather than linear layer theory. Error-field penetration, and subsequent locked mode formation, is triggered once the destabilizing effect of the resonant harmonic of the error-field overcomes the stabilizing effect of the ion polarization current (caused by the rotation of the error-field-induced island chain in the local ion fluid frame)—see section 3.2. The predicted scaling of the error-field penetration threshold with engineering parameters is $(b_r/B_T)_{crit} \sim n_e\, B_T^{-1.8}\, R_0^{-0.25}$, where $b_r$ is the resonant harmonic of the vacuum radial error-field at the resonant surface, $B_T$ the toroidal magnetic field-strength, $n_e$ the electron number density at the resonant surface and $R_0$ the major radius of the plasma—see section 4.3. This scaling—in particular, the linear dependence of the threshold with density—is consistent with experimental observations [5–8]. When the scaling is used to extrapolate from JET to ITER, the predicted ITER error-field penetration threshold is $(b_r/B_T)_{crit} \sim 5\times 10^{-5}$, which just lies within the expected capabilities of the ITER error-field correction system.

The analysis presented in this paper is based on a fluid approach that is, strictly speaking, only valid in a collisional plasma. At low collisionalities, such that $\nu_i \lesssim \epsilon_s\,\omega_{*i}$, which corresponds to (see sections 2.2, 4.1 and 4.2)

$$\frac{\bar{\nu}}{\rho_*} \lesssim \left(\frac{m_e}{m_i}\right)^{1/2} \frac{1}{\delta^3}, \tag{77}$$

the ion polarization term in the island width evolution equation is reduced by a factor $\epsilon_s^{3/2}$ [35, 36]. Moreover, the critical island width below which the polarization term ceases to vary as $w^{-3}$ becomes the ion banana width $\rho_b \sim (q_s/\epsilon_s^{1/2})\,\rho_s$, rather than $\rho_s$. However, neither of these modifications to the analysis would lead to a change in the predicted scaling of the error-field penetration threshold with engineering parameters.

## Appendix. Determination of $v_f$ and $I_p$

It is helpful to define the complete elliptic integrals

$$E(k) \equiv \int_0^{\pi/2} (1-k^2\,\sin^2 u)^{1/2}\,\mathrm{d}u, \tag{78}$$

$$K(k) \equiv \int_0^{\pi/2} (1-k^2\,\sin^2 u)^{-1/2}\,\mathrm{d}u. \tag{79}$$

Let

$$\langle 1\rangle \equiv K(1/k)/(k\,\pi), \tag{80}$$

$$\langle X^2\rangle \equiv (4k/\pi)\,E(1/k), \tag{81}$$

$$\langle X^4\rangle \equiv (16k/3\pi)\left[2\,(2k^2-1)\,E(1/k) - (k^2-1)\,K(1/k)\right] \tag{82}$$

for $k > 1$. As explained in [24], the parameter $v_f$ is calculated by solving the differential equation

$$0 \simeq \frac{\mathrm{d}}{\mathrm{d}k}\left[\frac{\langle X^4\rangle}{4k}\,d_k M + \left(1-\frac{1}{2}\,\frac{\tau_M}{\tau_P}\right)\frac{\langle X^4\rangle\langle 1\rangle}{\langle X^2\rangle^2}\right]$$

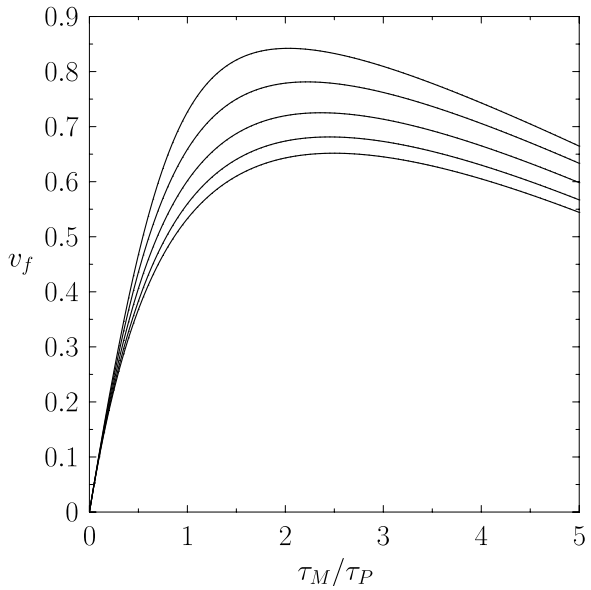


**Figure 6.** The phase velocity parameter, $v_f$, calculated as a function of the perpendicular diffusivity ratio, $\tau_M/\tau_P$. In order from the top to the bottom, the various curves correspond to $\tau = 0.25$, 0.5, 1.0, 2.0 and 4.0, respectively.

$$+\frac{1}{2}\,\frac{\tau_M}{\tau_P}\left(\frac{\langle X^4\rangle\langle 1\rangle}{\langle X^2\rangle^2}-1\right) \times \frac{[(1+2\tau)\,\langle X^2\rangle\,d_k M + \tau\,4k\,\langle 1\rangle/\langle X^2\rangle]}{\langle X^2\rangle\,M+\tau} \tag{83}$$

for $M(k)$ in the region $1 < k < \infty$, subject to the boundary conditions

$$M(k\to 1) \to (1-v_0)\,\frac{\pi}{4}, \tag{84}$$

$$M(k\to\infty) \to \frac{1-v_f}{2k}, \tag{85}$$

where

$$v_0 = \frac{(1+\tau)}{2}\left(1+\frac{\tau_M}{\tau_P} - \left[1-2\,\frac{\tau_M}{\tau_P}\left(\frac{1-\tau}{1+\tau}\right)+\left(\frac{\tau_M}{\tau_P}\right)^2\right]^{1/2}\right). \tag{86}$$

Here, $d_k \equiv \mathrm{d}/\mathrm{d}k$. Once the function $M(k)$ has been determined, the parameter $I_p$ is calculated from

$$I_p = \frac{2\pi}{3}\,v_0\,(1-v_0) - \int_1^\infty \frac{\langle X^2\rangle}{\langle 1\rangle}\left(\frac{\langle X^4\rangle\langle 1\rangle}{\langle X^2\rangle^2}-1\right) \times \left[d_k M\,(\langle X^2\rangle\,M-1) + \langle X^2\rangle\,M\,(d_k M + 4k\,\langle 1\rangle/\langle X^2\rangle^2)\right]\mathrm{d}k. \tag{87}$$

Figures 6 and 7 show $v_f$ and $I_p$ calculated, as described above, for various different values of the diffusivity ratio $\tau_M/\tau_P \equiv D_\perp/\mu_{\perp i}$ and the temperature ratio $\tau \equiv T_e/T_i$. The fact that $v_f$ is positive indicates that the island chain propagates in the electron diamagnetic direction relative to the local equilibrium ion fluid. Moreover, the fact that $I_p$ is positive indicates that the ion polarization current induced by this propagation has a stabilizing effect on the island chain.

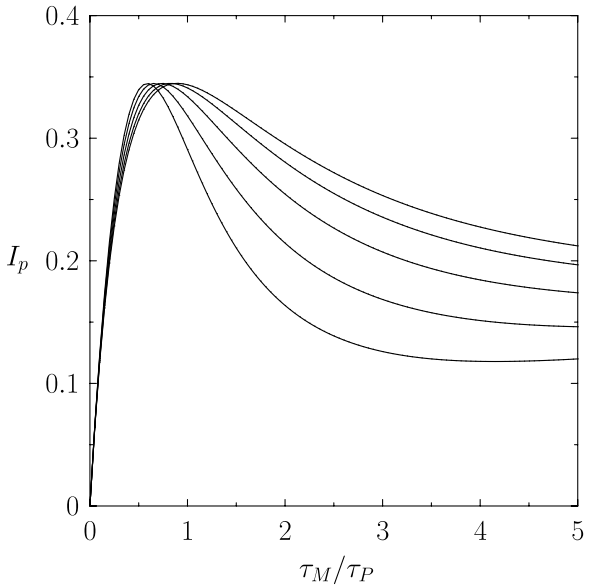


**Figure 7.** The ion polarization parameter, $I_{\rm p}$, calculated as a function of the perpendicular diffusivity ratio, $\tau_{\rm M}/\tau_{\rm P}$. In order from the bottom to the top, the various curves correspond to $\tau = 0.25$, 0.5, 1.0, 2.0 and 4.0, respectively.

## Acknowledgments

This research was funded by the US Department of Energy under contract DE-FG02-04ER-54742.

## References

[1] Wesson J A 2004 *Tokamaks* 3rd edn (Oxford: Oxford University Press)
[2] Scoville J T, La Haye R J, Kellman A G, Osborne T H, Stambaugh R D, Strait E J and Taylor T S 1991 *Nucl. Fusion* **31** 875
[3] Hender T C *et al* 1992 *Nucl. Fusion* **32** 2091
[4] Fishpool G M and Haynes P S 1994 *Nucl. Fusion* **34** 109
[5] Buttery R J *et al* , the JET Team, the COMPASS-D Research Team and the DIII-D Team 1999 *Nucl. Fusion* **39** 1827
[6] Buttery R J, De Benedetti M, Hender T C and Tubbing B J D 2000 *Nucl. Fusion* **40** 807
[7] Wolfe S M, Hutchinson I H, Granetz R S, Rice J, Hubbard A, Lynn A, Phillips P, Hender T C and Howell D F 2005 *Phys. Plasmas* **12** 056110
[8] Wolf R C *et al* and the TEXTOR Team 2005 *Nucl. Fusion* **45** 1700
[9] Boozer A H 2005 *Rev. Mod. Phys.* **76** 1071
[10] Chang Z and Callen J D 1990 *Nucl. Fusion* **30** 219
[11] Fitzpatrick R 1993 *Nucl. Fusion* **33** 1049
[12] Fitzpatrick R 1998 *Phys. Plasmas* **5** 3325
[13] Connor J W and Taylor J B 1977 *Nucl. Fusion* **17** 1047
[14] Shimada M *et al* 2007 *Nucl. Fusion* **47** S1
[15] Hender T C *et al* and the ITPA MHD, Disruption and Magnetic Control Topical Group 2007 *Nucl. Fusion* **47** S128
[16] Pfeiffer W W and Waltz R E 1979 *Nucl. Fusion* **19** 51
[17] Goldston R J 1984 *Plasma Phys. Control. Fusion* **26** 87
[18] Cole A and Fitzpatrick R 2006 *Phys. Plasmas* **13** 032503
[19] Cole A J, Hegna C C and Callen J D 2008 *Phys. Plasmas* **15** 056102
[20] Shaing K, Hirshman S and Callen J D 1986 *Phys. Fluids* **29** 521
[21] Shaing K 1993 *Phys. Fluids* B **5** 3841
[22] Shaing K 2003 *Phys. Plasmas* **10** 1443
[23] Fitzpatrick R and Waelbroeck F L 2008 *Phys. Plasmas* **15** 012502
[24] Fitzpatrick R and Waelbroeck F L 2010 *Phys. Plasmas* **17** 062503
[25] Morris R C, Haines M G and Hastie R J 1996 *Phys. Plasmas* **3** 4513
[26] Furth H P, Killeen J and Rosenbluth M N 1963 *Phys. Fluids* **6** 459
[27] Rutherford P H 1973 *Phys. Fluids* **16** 1903
[28] Rutherford P H 1986 *Basic Physical Processes of Toroidal Fusion Plasmas, Proc. Course and Workshop (Varenna, Italy 1985)* vol 2 (Brussels: Commission of the European Communities) p 531
[29] Smolyakov A I 1993 *Plasma Phys. Control. Fusion* **35** 657
[30] Waelbroeck F L and Fitzpatrick R 1997 *Phys. Rev. Lett.* **78** 1703
[31] Carrera R, Hazeltine R D and Kotschenreuther M 1986 *Phys. Fluids* **29** 899
[32] Kotschenreuther M, Hazeltine R D and Morrison P J 1985 *Phys. Fluids* **28** 294
[33] ITER Physics Basis Editors 1999 *Nucl. Fusion* **39** 2175
[34] Simmet E E and the ASDEX Team 1996 *Plasma Phys. Control. Fusion* **38** 689
[35] Poli E, Bergmann A and Peeters A G 2005 *Phys. Rev. Lett.* **94** 205001
[36] Imada K and Wilson H R 2009 *Plasma Phys. Control. Fusion* **51** 105010